

# Numerical modelling of a centrifuged embankment on soft clay

M. S. S. ALMEIDA

*COPPE—UFRJ, Post Graduation School, Federal University of Rio de Janeiro, P.O. Box 68506, 21944, Rio de Janeiro RJ, Brazil*

AND

A. M. BRITTO AND R. H. G. PARRY

*Engineering Department, Cambridge University, Trumpington Street, Cambridge, United Kingdom CB2 1PZ*

Received July 12, 1985

Accepted November 27, 1985

Biot coupled consolidation numerical analyses have been applied to a stage-constructed embankment on soft clay in the centrifuge. In the test, the sand embankment was constructed during flight on a clay foundation consisting of an overconsolidated crust overlying a normally consolidated layer. Measurements were taken of pore pressures, dissipation rates, and displacements in the foundation clay. Predictions of these were made using a simple Cam-clay model for the clay and the Cambridge CRISP computer program. A linear elastic idealization was used for the embankment. With some exceptions, pore pressures and dissipation rates were very well predicted, as were maximum values of both horizontal and vertical displacements. However, displacement profiles with depth were not so well predicted. Particular attention is given in the paper to the determination of relevant values of shear modulus  $G$  and the difference in behaviour resulting from using constant permeability and permeability varying with void ratio.

*Key words:* embankments, soft clay, centrifuge test, numerical analysis, Biot consolidation, Cam-clay model.

Des analyses numériques associées à la théorie de consolidation de Biot ont été appliquées à un remblai sur argile molle construit par étapes dans un centrifuge. Le remblai en sable a été construit durant l'essai sur une fondation argileuse comprenant une croûte surconsolidée recouvrant une couche normalement consolidée. Des mesures de pressions interstitielles, de vitesses de dissipation et de déplacements dans la fondation argileuse ont été prises. Des prédictions de ces mesures ont été faites au moyen d'un simple modèle "Cam-clay" pour l'argile et du programme d'ordinateur CRISP de Cambridge. Le comportement du remblai a été idéalisé selon un modèle d'élasticité linéaire. À quelques exceptions près, les pressions interstitielles et les vitesses de dissipation ont été très bien prédites de même que les valeurs maximales des déplacements horizontaux et verticaux. Cependant, les profils de déplacements en fonction de la profondeur n'ont pas été aussi bien prédits. Dans cet article, une attention particulière est portée à la détermination des valeurs du module de cisaillement  $G$ , et au comportement différent selon qu'une perméabilité constante ou variant avec l'indice des vides est utilisée.

*Mots clés:* remblais, argile molle, essai centrifuge, analyse numérique, consolidation de Biot, modèle "Cam-clay."

[Traduit par la revue]

Can. Geotech. J. 23, 103–114 (1986)

## Introduction

Realistic computations of the variation of displacements and pore pressures with time, in clay foundations under stage-constructed embankments, require the use of numerical analyses with reliable constitutive models coupled with consolidation.

The Cam-clay models (Schofield and Wroth 1968; Roscoe and Burland 1968) allow strength and compressibility to be treated within the elastoplastic strain-hardening theoretical framework, using a small number of parameters for both drained and undrained analyses. Partial drained behaviour can be also modelled numerically using the Biot three-dimensional consolidation theory, as adopted in the CRISP program (Gunn and Britto 1981). Some common criticisms (e.g. Tavenas 1981) to the original Cam-clay models are the following:

- (a) the assumption of a yield locus centred on the isotropic compression line whereas anisotropic consolidated clays exhibit yield loci approximately centred on the  $K_0$  consolidation line (e.g. Parry and Nadarajah 1973);
- (b) the assumption of isotropic elastic rather than anisotropic elastic behaviour inside the yield locus;
- (c) the assumption of associated flow rules, which can be acceptable for isotropic soils but do not properly represent the behaviour of anisotropic natural clays.

Despite the above criticisms, the original Cam-clay models have been continuously used at Cambridge. The reasons are that they retain mathematical simplicity and use a small set of parameters obtainable from standard laboratory tests.

This paper is concerned with comparisons between numerical

calculations of pore pressures and displacements and measurements taken during the centrifuge testing of a stage-constructed embankment on soft clay.

## Centrifugal modelling

The advantages of using the centrifuge to achieve self-weight and stress path similarity have been discussed by Schofield (1980). In essence, if a model  $N$  times smaller than the prototype is subject to an acceleration  $N$  times the earth's gravity field, then the density of all materials in the model will be increased by  $N$  and the stresses at a depth  $z$  will be identical to the stresses in the prototype at a depth  $z$ . If materials with the same stress-strain behaviour are used in both model and prototype, strain similarity is also achieved in both model and prototype.

An additional advantage of a centrifuge test is the shortening of time-dependent processes. According to the Terzaghi consolidation theory, the time for dissipation of excess pore pressure is proportional to the square of the drainage path. As the model dimensions are reduced by  $N$  times, the drainage path is also  $N$  times shorter. Hence the model time is  $N^2$  times shorter than the prototype time. This relation has obvious implications for the centrifuge modelling of stage-constructed embankments on soft clays.

The centrifuge test reported here is part of an extensive programme of testing carried out at Cambridge to study the behaviour of embankments on soft clays (Davies 1981; Almeida 1984; Almeida *et al.* 1985; Davies and Parry 1985). The model

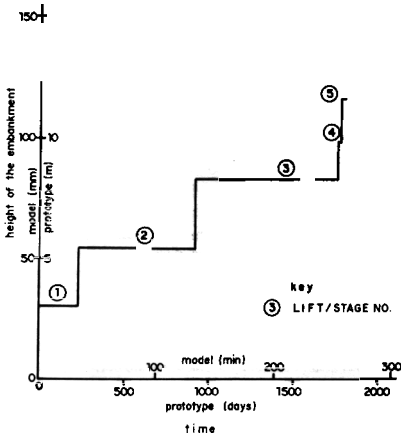


Fig. 1. Construction history for stage-constructed embankments.

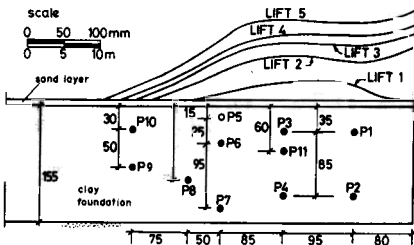


Fig. 2. Centrifuge test MA3: geometry and position of the pore pressure transducers.

test (Almeida 1984) consisted of a 160 mm thick soft clay foundation formed by a 90 mm overconsolidated clay overlying a 70 mm normally consolidated layer. In order to produce a stiff crust, Gault clay was used in the top 40 mm of the model. Both clays were consolidated together from slurry. The *in situ* stress state existing before embankment construction is described below.

The centrifuge test was performed at 100 *g* using the Cambridge geotechnical centrifuge described by Schofield (1980). Embankments were constructed in flight; the stage construction loading history that was adopted during the centrifuge test and that is to be modelled numerically is shown in Fig. 1. The embankment was constructed in stages from lift 1 to lift 3 and was then taken quickly to failure. This occurred 10 s after lift 5 was poured, at an average height of 116 mm.

The geometry of the problem is seen in Fig. 2. Since the walls of the centrifuge container are ideally smooth, the cross section of the model represents half of the prototype modelled, as the right-hand-side wall is a plane of symmetry. The positions of the 10 miniature pore pressure transducers used are also seen in Fig. 2. As the pore pressure transducers were provided with silicon chips, they offer very fast response times, of the order of 0.1 s. The visible section of the model was provided with a grid of

silver spheres that allowed pictures to be taken and displacements to be subsequently computed, by the technique described by James (1973).

During stages 2 and 3 of embankment construction large horizontal and vertical displacements occurred. Measured and computed displacements and pore pressures are presented below. Limit equilibrium effective stress stability analyses using measured pore pressures produced factors of safety in the range 1.0–1.2 during stages 2 and 3 and a factor of safety of 0.91 at failure, as described by Almeida *et al.* (1985). A full description of the test, techniques, and analyses performed can be found in Almeida (1984).

### Previous work on critical state numerical modelling

One strong feature of the Cam-clay models is their ability to model the behaviour of lightly overconsolidated clays under stress paths corresponding to embankment loading (Wood 1982). Indeed, Cam-clay models have been successfully used (e.g. Wroth 1977) for the numerical calculations of the behaviour of embankments on clay foundations. A brief review of prior numerical analyses of embankments on soft clays using critical state models is presented below.

The finite element program developed by Simpson (1973) employing models of soil behaviour and based on critical state soil mechanics was applied to the analysis of the Kings Lynn trial embankment. Drained and undrained analyses showed good agreement for short- and long-term settlements. Computed pore pressure showed less agreement with field measurements than displacements and poor agreement was obtained between measured and computed movements outside the embankment toe. The results of these analyses were also presented by Wroth and Simpson (1972). Thompson (1976) improved Simpson's program and applied it to a class A prediction of the MIT trial embankment. The calculations were good in general, but pore pressure computations in particular were better than those presented by the other predictors (Wroth 1977).

From the findings of Simpson, Thompson, and others (notably Naylor 1975), the CRISTINA (CRITICAL STATE Numerical Algorithm) program was developed. Bassett *et al.* (1981) used a version of CRISTINA with a coupled consolidation algorithm suggested by Small *et al.* (1976) to predict the behaviour of centrifuged constructed embankments. Davies (1981) used CRISP, the version subsequent to CRISTINA, and described in the next section, for the analysis of centrifuged embankments. In both cases excess pore pressures generated by the embankment construction and their rates of dissipation were fairly well predicted, but the settlements during consolidation were substantially overpredicted, with a much deeper pattern of computed displacements.

Prediction of the behaviour of a trial embankment on Rio de Janeiro clay was performed by Almeida (1981) using the CRISP program. A coupled consolidation analysis of the month-long period was performed and good agreement was observed for both settlements and pore pressures. When results were also compared (Almeida and Ortigão 1982) with numerical calculations using an elastic nonlinear model, the superiority of critical state numerical calculations that accounted for the soil consolidation was made evident.

Other critical state finite element programs have been developed elsewhere, such as the Rosalie program used for predictions of the Cubzac-les-Ponts A and B trial embankments (Truong and Magnan 1977; Magnan *et al.* 1982a, b). Early

analyses without consolidation (Truong and Magnan 1977) were sensitive to the *in situ* value of  $K_0$  adopted and settlements were generally underestimated. The program has recently been modified (Magnan *et al.* 1982a, b) to include coupled consolidation, yield locus centred on the  $K_0$  line, anisotropic elastic behaviour inside the yield locus, and nonassociative flow rule, to give, consequently, better results.

Numerical analyses of the 1-95 MIT test embankment and of the East Aichafalaya test section were presented by Kavazanjian and Poepel (1984). Agreement between observed and computed values was generally satisfactory, after soil parameter calibration upon initial construction deformations. Underprediction of both lateral deformations and center-line settlements was attributed to undrained creep, which is not included in the numerical modelling.

### CRISP program and finite element mesh used

Constitutive models included in CRISP are Cam-clay, elastic perfectly plastic, and linear elastic. The clay foundation has been modelled here as a modified Cam-clay material (Roscoe and Burland 1968) and the soil parameters adopted are presented in the next section. A study of the suitability of the models available in CRISP to be used for the embankment was performed by Almeida (1981). It was concluded that despite its shortcomings the linear elastic model was the most convenient; thus it is adopted here for both embankment and sand layer. Values adopted for Young's modulus were  $E = 3$  MPa for the embankment and  $E = 2$  MPa for the sand layer, based on correlations with cone penetration tests performed through the embankment and top sand layer during centrifuge operation (Almeida 1984). A Poisson's ratio of  $\nu' = 0.3$  was adopted for both materials.

Triangular and quadrilateral elements with displacements unknown, or with both pore pressure and displacements unknown are provided in the program. The six-noded triangle (Fig. 3a) was used to model the consolidating clay foundation. The sand layer and the embankment were modelled as drained materials and the element types used have only displacement unknown at the nodes (Fig. 3b, c).

The finite element mesh with the type of elements mentioned above is presented in Fig. 4. It is composed of a total of 130 elements, 85 being in the clay foundation, 12 in the sand layer, and 33 in the embankment. The embankment consisted of four lifts, lift 5 being simulated by distributed load on the top of lift 4. The total number of nodes in the mesh was 319 and the maximum number of degrees of freedom in the solution (after constructing lift 4) was 694.

The formulation of consolidation is based on Biot's three-dimensional consolidation theory. Physical nonlinearity is handled by a purely incremental approach, which requires the use of a larger number of increments.

Boundary conditions adopted in the analysis, Fig. 4, are those existing inside the centrifuge model container and consist of sides restrained horizontally but allowed to move vertically, and bottom restraint in both horizontal and vertical directions. Drainage was permitted at the top and bottom of the clay model throughout the analysis, i.e., during both loading and consolidation.

The analysis was performed by applying onto the mesh the embankment self-weight under centrifuge acceleration for each lift, and allowing for partial pore pressure dissipation under that load. The bulk specific weight of the embankment was  $16.9 \text{ kN/m}^3$ . All the elements corresponding to the embank-

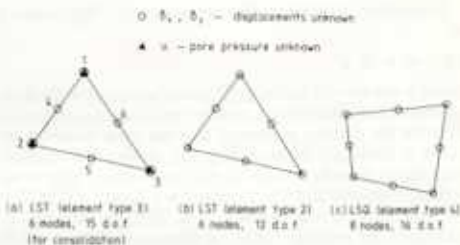


FIG. 3. Types of elements used

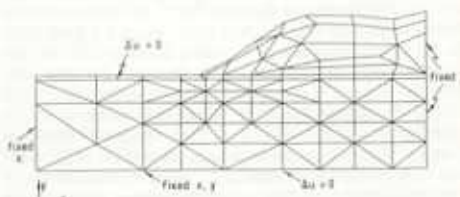


FIG. 4. Finite element mesh and boundary conditions.

ment material were removed prior to analysis. Times for both loading and consolidation were exactly the same as in the centrifuge test.

### Modelling the clay foundation

#### Critical state parameters

The Cam-clay model requires four critical state parameters:  $\lambda$ , the gradient of the consolidation line in the  $e - \ln p'$  space, equal to  $C_c/2.3$ ;  $\kappa$ , the gradient of the swelling line in the  $e - \ln p'$  space, equal to  $C_s/2.3$ ;  $M$ , the value of the stress ratio  $q'/p'$  at the critical state condition; and  $e_{cs}$ , the void ratio at  $p' = 1 \text{ kPa}$  on the critical state line in the  $e - \ln p'$  space.

The following values adopted in the analyses were based on the large amount of data available at Cambridge (e.g. Airey 1984; Davies 1981; Parry and Nadarajah 1973; Thompson 1976): kaolin:  $\lambda = 0.25$ ,  $\kappa = 0.05$ ,  $M = 0.9$ ,  $e_{cs} = 2.44$ , Gaul clay:  $\lambda = 0.219$ ,  $\kappa = 0.035$ ,  $M = 1.0$ ,  $e_{cs} = 1.96$ .

#### Shear moduli

The matrix of elastic components is computed in the CRISP program using values of shear modulus  $G$  and bulk modulus  $K'$ . The bulk modulus is pressure dependent and is computed by differentiating the equation of a swelling line.

$$[1] \quad K' = \frac{(1 + e)p'}{\kappa}$$

When using the standard version of the program it is possible to assign either a constant value of shear modulus or a constant value of Poisson's ratio. It appears that neither of the assumptions of  $G$  or  $\nu'$  constant is satisfactory, as discussed below. In the latter case the shear modulus is pressure dependent and given by

$$[2a] \quad G = \frac{3(1 - 2\nu')}{2(1 + \nu')} K'$$

Substituting values of  $e = 1.5$ ,  $\kappa = 0.05$ , and  $\nu' = 0.3$  gives

$$[2b] \quad G = 23 \cdot p'$$

Triaxial tests in kaolin carried out by Houlsby (1981) resulted

$$[3] \quad G = 75 \cdot p'$$

Houlsby also showed that using [3] provided a much better fit to his triaxial tests than using a constant value of shear modulus. Thus for the analysis performed here the shear modulus for kaolin is constantly updated using [3], despite this equation implying an unrealistic value of zero for Poisson's ratio when [1] and [3] are substituted in [2a] with  $e = 1.5$  and  $\kappa = 0.05$ . For the Gault clay,  $G$  was assumed to be 2250 kPa (see Fig. 5) throughout the analysis. Values of  $G$  corresponding to the *in situ* stress state,  $p = (2\sigma'_{ho} + \sigma'_{vo})/3$ , are shown in Fig. 5.

Values of  $G$  computed by [2a] (making the normal assumption of  $\nu' = 0.3$ ) are also shown in Fig. 5, and are much lower than those given by [3]. The ratio  $G/c_u$ , which is a good guide for the estimated values of  $G$ , varies between 130 and 230 (Houlsby 1981), as shown in Fig. 6. However, the same ratio given by values of  $G$  computed by [2a] varies between 27 and 74, Fig. 6, whereas that using values of  $G$  computed by [3] varies between 72 and 270, Fig. 6. Thus values of  $G$  for kaolin given by [3] seem to be quite realistic, whereas use of [2] might lead to excessively low values of  $G$ , which might explain why some previous critical state numerical analyses overpredicted displacements.

*Coefficients of permeability*

For coupled consolidation analysis the program also requires values of the coefficients of permeability in the horizontal ( $k_h$ ) and vertical ( $k_v$ ) directions. In the standard version of CRISP the coefficient of permeability is assumed to remain constant throughout the analysis.

However, the permeability is not a soil constant and in situations in which large loads are applied and significant consolidation takes place, changes in void ratio can lead to important changes in the coefficient of permeability. This point might be important in stage-constructed embankments and is investigated here; two cases have been analysed:

(a) *Case A*—The permeability was assumed to be dependent on the void ratio; this case was used for direct comparison with the observed behaviour. Four values of the initial coefficient of permeability in the vertical direction ( $k_{v0}$ ) were used. Fig. 7b, according to the initial void ratio  $e_0$ , Fig. 7a. The equation adopted to correlate the coefficient of permeability with the void ratio in case A and which was implemented in the original version of the CRISP program is the linear relationship between  $\log k_v$  and  $e$  given by

$$[4] \quad k_v = k_{v0} \cdot 10^{(e - e_0)/C_k}$$

where  $k_{v0}$  and  $e_0$  have been defined above and  $C_k$  is the slope of the  $\log k_v - e$  plot. The value of  $C_k$  adopted for both kaolin and Gault clay was 0.60, which, like  $k_{v0}$ , was based on data available at Cambridge (Thompson 1962);

(b) *Case C*—The permeability was assumed to remain constant throughout the analysis; this case was used just for comparison with case A. Only two values of permeability were used (Fig. 7b):  $k_v = 9.37 \times 10^{-10}$  m/s for the Gault clay and  $k_v = 2.0 \times 10^{-9}$  m/s for the entire kaolin clay layer.

In both cases values of  $k_h$  were assumed to be 1.5 times higher than those of  $k_v$ , according to experimental data available at Cambridge (Chan 1975).

*In situ stress state*

A soil element close to the clay surface (see Fig. 8b, element A), in clay models used for centrifuge tests, experiences loading

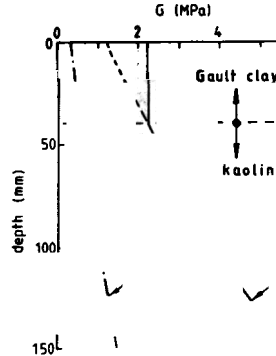


FIG. 5. Variation of shear modulus with depth.

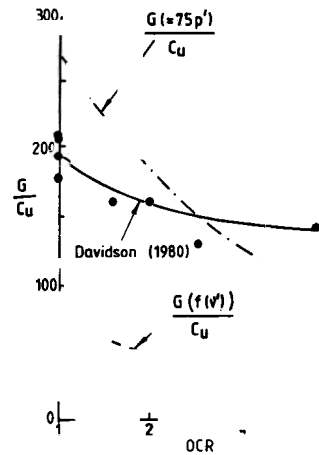


FIG. 6. Variation of  $G/c_u$  with OCR.

in the laboratory and continuous swelling as it is unloaded and then subjected to 100 g of acceleration, eventually reaching equilibrium. On the other hand, a soil element at the bottom of the clay (see Fig. 8b, element B) experiences loading followed by unloading and subsequent reloading to a normally consolidated condition as it reaches equilibrium at  $N = 100$  g.

Values of *in situ* horizontal effective stresses  $\sigma'_{ho}$  were computed using values of coefficients of earth pressure at rest  $K_0 = \sigma'_{ho}/\sigma'_{vo}$  given by the following empirical relationship found to be suited to Cambridge reconstituted clays:

$$[5] \quad K_0 = K_{nc} \cdot (\text{OCR})^{\phi} \text{ (radians)}$$

where  $\text{OCR} = \sigma'_{vm}/\sigma'_{vo}$  is the overconsolidation ratio and  $K_{nc}$  is the coefficient of earth pressure at rest at the normally consolidated condition, equal to 0.69 for both kaolin and Gault clay (Airey 1984; Thompson 1962). Results from [5] agree well with the available experimental data.

Variations of OCR and  $K_0$  (given by [5]) with depth in the clay foundation are given in Fig. 8a. Values of *in situ* vertical

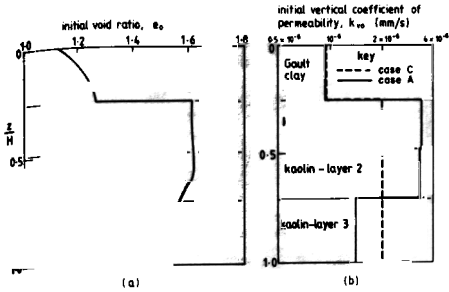


FIG. 7. Distribution of void ratio and permeability in clay foundation.

and horizontal effective stresses  $\sigma'_{vo}$  and  $\sigma'_{ho}$  are shown in Fig. 8b. The bulk specific weight of the clay foundation was  $15.4 \text{ kN/m}^3$ . The third curve in Fig. 8b is the isotropic preconsolidation pressure  $p'_c$  required by Cam-clay models to locate the yield locus at each integration point. Values of  $p'_c$  have been computed from the stress history ( $\sigma'_{ho}$ ,  $\sigma'_{vo}$ , and OCR) using the equation of the modified Cam-clay yield locus.

**Predicted and measured displacements**

**Results**

Predicted vertical displacements at the top of the clay surface and displacements measured 5 mm (0.5 m) below the clay surface (there were practical difficulties of positioning the reflective markers used for displacement measurements at the clay surface) are compared in Figs. 9a–9c. Plots are given at moments shortly after lift 2 was placed and just before lift 3 was placed (i.e. start and end of stage 2), Fig. 9a; at start and end of stage 3, Fig. 9b; and just after construction of lift 5. Magnitudes of both settlement under the embankment and heave in front of the embankment are generally very well computed.

As far as surface settlements are concerned, the only factor of discrepancy is related to the shape of the curves under the embankment. It is believed that side friction developing inside

the centrifuge model container is of minor importance and that the modelling of the embankment as an elastic material is the main reason for the difference, as discussed in detail by Almeida (1984). Indeed, back analysis of the embankment failure (Almeida *et al.* 1985) using well-known effective stress strength parameters and measured pore pressures produced a factor of safety of 0.91, thus suggesting that side friction, not considered in the stability analysis, was less than 10%. Also, use of an embankment with very low stiffness, although overpredicting displacements, produced a displacement profile similar to the observed one, suggesting that the use of a stress-dependent embankment modulus should improve the results.

The variation of settlements with time is shown in Fig. 10 for a point 22.5 mm (22.5 m) away from the embankment centre line. The few data regarding the variation of settlement with time suggests that this is being well computed. However, the variation of settlements with depth is not as well computed as surface settlements, Fig. 11, since computed displacements decrease gradually with depth, with displacements at great depths being greatly overpredicted. The reason for this discrepancy is not clear.

Equivalent inclinometer plots I1, I2, and I3 are presented in Figs. 12 and 13 for lifts 2, 3, and 5. Maximum horizontal displacements are well predicted at inclinometers I1 and I3 but not so well at inclinometer I2. Maximum computed horizontal displacements were located at a depth ratio  $z/H$  of the order of 0.24–0.4, whereas observed maximum values were at a depth ratio of the order of 0.0–0.2. Similar to the vertical displacements, observed horizontal displacements had a more pronounced gradient with depth than computed values; hence displacements at great depth were overpredicted.

Contours of computed vertical and horizontal displacements at the end of stage 3 are presented in Figs. 14a and 14b. The general agreement in magnitude between calculations and measurements but the deeper pattern of computed displacements can be seen by comparing the calculations of Fig. 14 with measurements presented in Fig. 15.

**Discussion**

Maximum magnitudes of both heave in front of the embankment and settlements under the embankments were very well

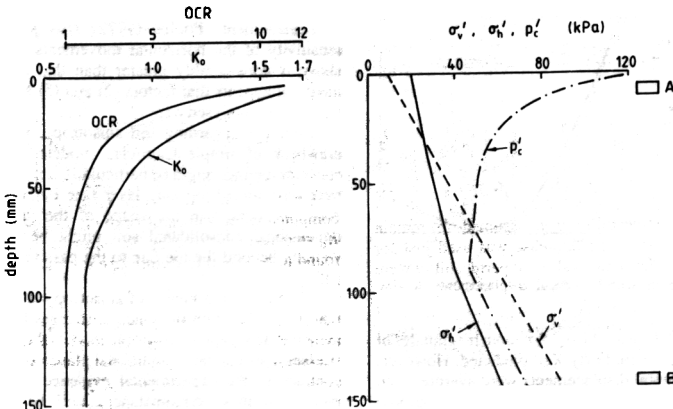


FIG. 8. *In situ* stress state.

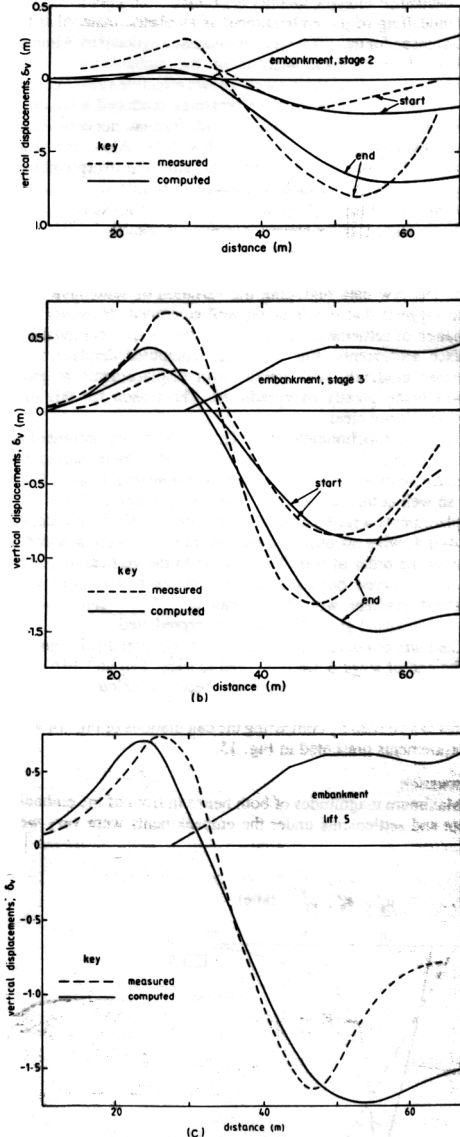


FIG. 9. Computed and measured vertical displacements at clay surface.

predicted at all stages of the test. Also, maximum magnitudes of horizontal displacements were fairly well predicted. However, both vertical and horizontal displacements were overpredicted at greater depths. Computed horizontal displacements appeared to be restrained at the clay surface, thus differing in shape from the measured curves. Difficulties associated with calculations of

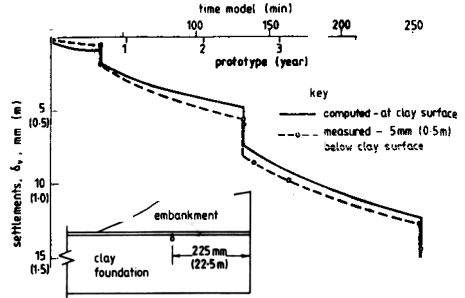


FIG. 10. Computed and measured settlements with time.

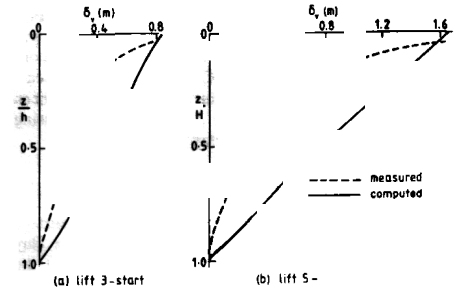


FIG. 11. Computed and measured settlements with depth.

lateral deformations of foundations were discussed by Poulos (1972). Predicted horizontal displacements are usually larger than measurements and Poulos listed the possible reasons for the discrepancies: (1) the difficulty of estimating Poisson's ratio of the soil; (2) anisotropy of the soil; (3) nonlinear stress-strain behaviour of soil; (4) nonhomogeneity of soil; (5) neglect of certain factors such as the effect of embankment stiffness and foundation roughness or more generally, incorrect assumptions made regarding the stresses applied to the soil by the foundation or embankment. Poulos (1972) also pointed out that the sensitivity of the horizontal movements to the factors listed above is considerably greater than that of vertical displacements. It appears that factors (2) and (5) are the most relevant for the case analysed here.

Factor (2), regarding soil anisotropy, is possibly the main drawback of simple Cam-clay models. Indeed, anisotropic elastic behaviour might be particularly important for the initially overconsolidated top clay layer (see Parry and Wroth 1977). Also, anisotropy in the shape of the yield locus for one-dimensional consolidated soil might be relevant for points yielding beyond the toe due to the passive nature of the stress paths.

Related to the influence of anisotropy is the problem of rotation of the direction of principal stresses beyond the embankment toe. In Cam-clay isotropic models the rotation of principal stresses does not cause additional plastic strains, which is quite contrary to the experimental evidence. Therefore Cam-clay models in these circumstances will be too stiff and will underpredict deformations. This is the case for lateral deformations of points close to the surface in equivalent inclinometers II

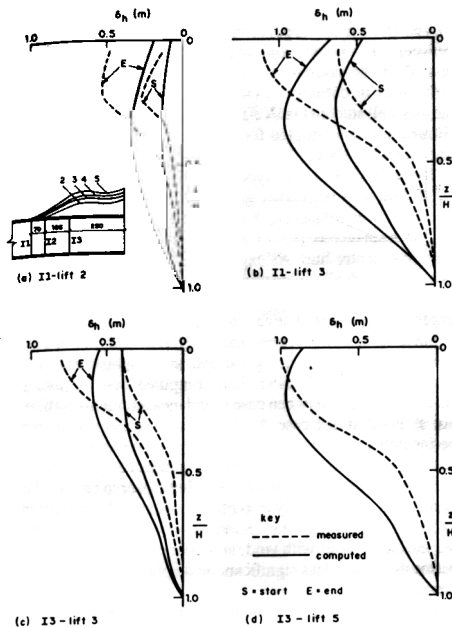


FIG. 12. Equivalent inclinometer plots I1 and I3—computed and measured displacements.

and I2. However, the opposite occurs in the bottom clay layer, which is yielding more than expected, i.e. plastic strains and displacements are being overpredicted there.

The modelling of the embankment also seemed to be unsatisfactory, as suggested in (5) above, as a linear elastic model does not model the variation of the embankment stiffness with stress level. Therefore it is apparent that a more correct modelling of the embankment material should improve the shape of the settlement curves under the embankment and the profiles of lateral deformations and settlement with depth.

The discussion by Poulos (1972) was made in the context of a quickly built embankment. In the case of a stage-constructed embankment, the hypotheses regarding the consolidation of the clay foundation might also be important. It was observed in the analyses performed here that the assumption of permeability being constant throughout the analysis (case C) has the effect of increasing lateral deformations and settlements as compared to the assumption of permeability varying with void ratio (case A).

#### Predicted and measured pore pressures

Excess pore pressures  $\Delta u$  measured during test MA3 are compared in this section with values of  $\Delta u$  computed at the integration point nearest to the respective pore pressure transducer.

Measured and computed variations of excess pore pressure with time are presented in Figs. 16 and 17 for 8 of the 10 transducers monitored. The agreement is generally good for both generation and dissipation of pore pressures. Computed pore pressures had a trend of peaking at the end of loading whereas measured pore pressures showed some peak delay, i.e.

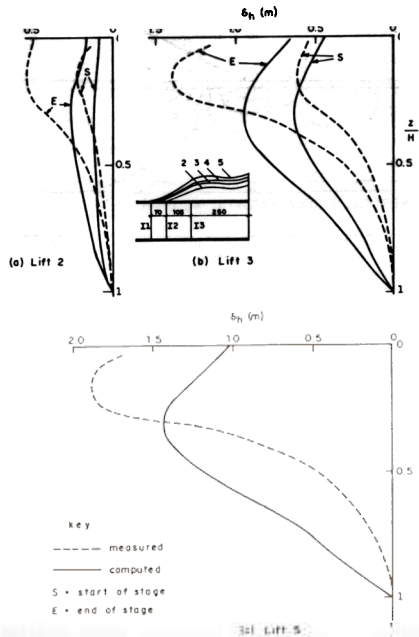


FIG. 13. Equivalent inclinometer plot I2—computed and measured displacements.

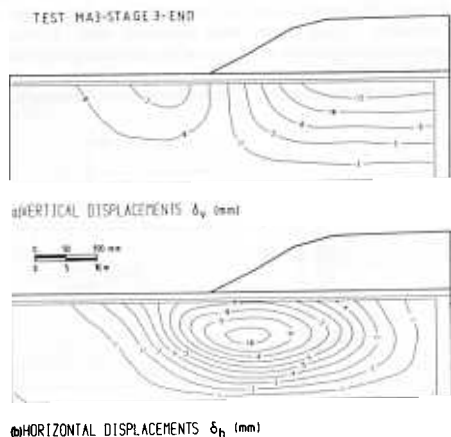


FIG. 14. Computed vertical and horizontal displacements.

peaked after the end of loading. That is the case of transducer P6, Fig. 16c, where, despite the poor agreement, both computed and measured pore pressures peaked on completion of loading lifts 1–3.

At transducer P9, Fig. 17b, computed pore pressures showed a continuous rise on completion of loading lift 1,

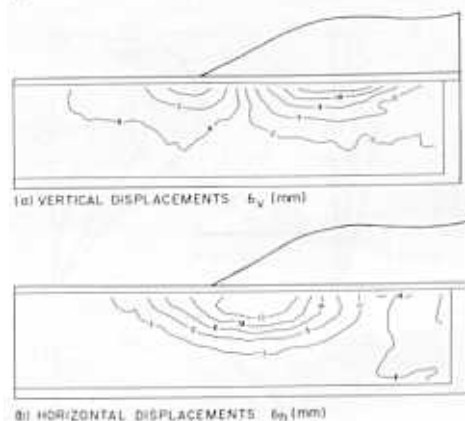


FIG. 15. Measured vertical and horizontal displacements.

maximum values being obtained at the end of the stage. Also, at transducer P10, Fig. 17c, computed  $\Delta u$  remained stable for some time at the beginning of stages 2 and 3, which was also the case for the early moments of stage 2 in transducer P11, Fig. 17d. The delayed peak response as well as the continuous rise in pore pressure at the end of loading may be a consequence of both the two-dimensional pore pressure redistribution in the clay foundation and the Mandel-Cryer effect (Gibson *et al.* 1963), which are also reflected in the computational method.

Transducers located in the Gault clay (P1 and P10) or close to the interface between Gault clay and kaolin (P6 and P11) showed, for some stages of the tests, computed rates of dissipation slightly faster than measured ones. However, computed pore pressure responses at the remaining transducers located within kaolin were generally very good, and particularly noticeable are the excellent agreements obtained for transducers

P2 and P9. Thus it appears that the few existing discrepancies between calculations and measurements are not particularly related to the computational model adopted but rather with difficulties in defining exactly the consolidation properties of the less well studied Gault clay. If lower values of coefficients of permeability are adopted for Gault clay, the predicted dissipation should improve.

The influence of the hypotheses regarding variation of the coefficient of permeability given by cases A and C is shown in Fig. 18. Comparisons are made for transducers P2, P3, P6, and P9, at respectively 8, 17.5, 26, and 35 m away from the prototype centre line. As expected, the difference between the two cases gradually increases for points closer to the centre line, as these are subjected to greater overburden pressures, hence experiencing larger changes in void ratio.

Since agreement between measurements and case A calculations was generally very good and as computed case C pore pressures dissipated faster than computed case A pore pressures, agreement between case C and measurements is therefore not as good as for case A. Analysis for a case in which the permeability was kept constant throughout the analysis but with initial distribution as in case A produced pore pressures intermediate between cases A and C but closer to case C. Thus it appears that it is not only important to assume the correct initial values of  $k_{in}$  and  $k_{out}$ , but even more important to assume that the permeability varies with void ratio. The effect of the variation of permeability was less significant on displacements than on pore pressures.

Contours of computed  $\Delta u$  at the end of stage 3 are shown in Fig. 19. Values presented a decrease of  $\Delta u$  from mid-depth to top and bottom draining boundaries and from the prototype centre line to the embankment toe, as expected.

#### Stress distribution on the clay foundation

Computed stress paths in the  $p^*-q^*$  diagram plotted at the location of the pore pressure transducers P1, P2, P7, P8, P10, and P11 are shown in Fig. 20, where  $q^*$  is the generalized deviator stress as defined by Roscoe and Burland (1968). The

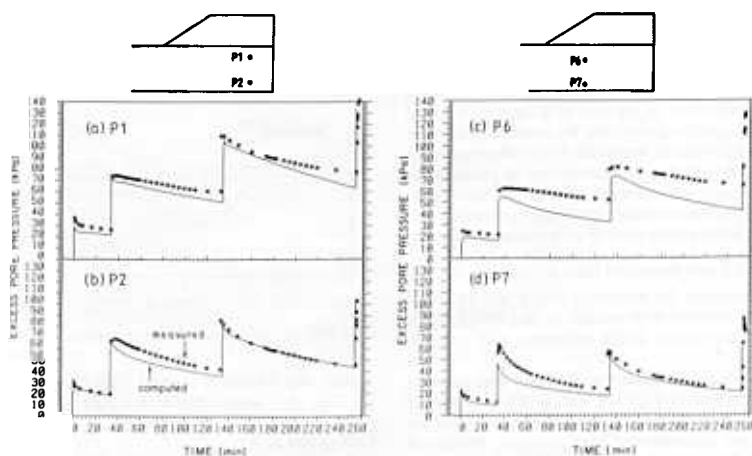


FIG. 16. Measured and computed pore pressure, transducers P1, P2, P6, and P7.

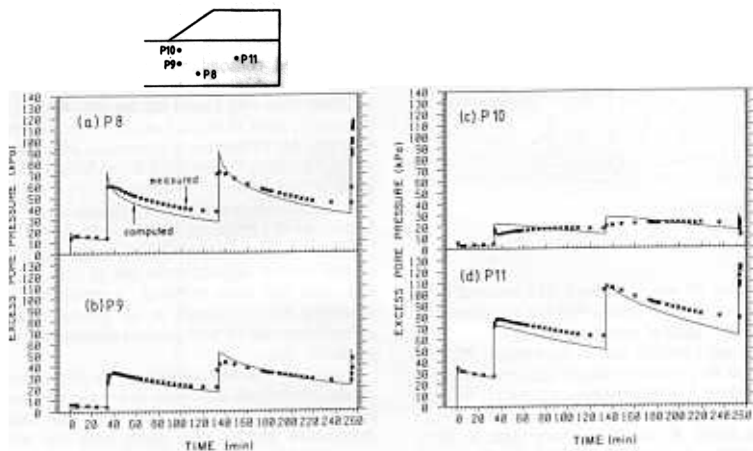


FIG. 17. Measured and computed pore pressures at transducers P8, P9, P10, and P11.

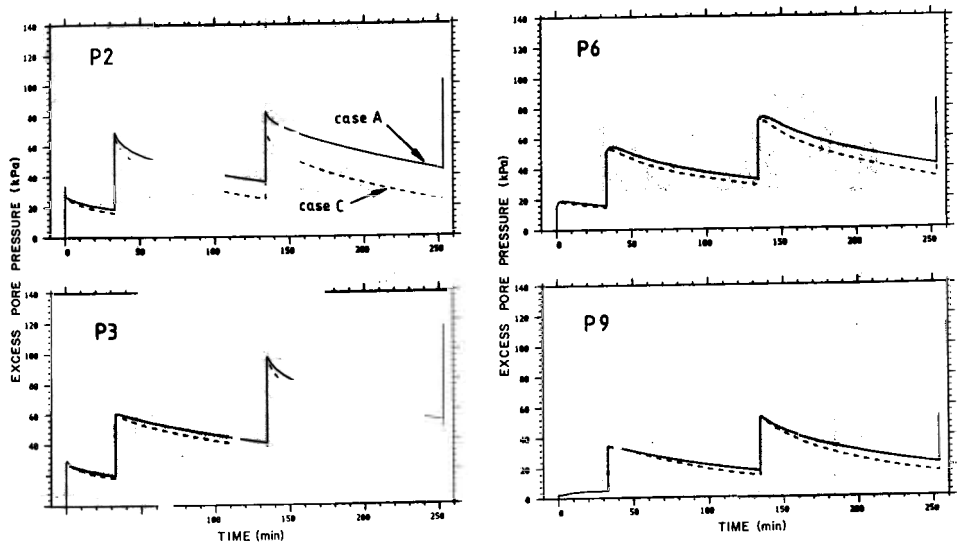


FIG. 18. Influence of the hypothesis related to the permeability on the pore pressure response.

critical state line (csl) and the modified Cam-clay yield locus are also plotted in the  $p'$ - $q^*$  diagram.

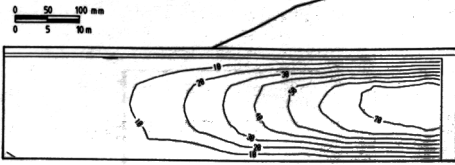
Points P1, P10, and P11 are located in the top overconsolidated clay layer, thus stress paths at these points start inside the yield locus. Conversely, points P2, P7, and P8 are in the bottom normally consolidated layer and their stress paths initiate on the yield locus. Stress paths shown in Fig. 20 may be described as follows:

(a) During loading, undrained type of stress path, vertical for

points at the overconsolidated state and inclined to the left for points at the normally consolidated state, which is consistent with the negligible drainage taking place during the short time of construction. These stress paths generally moved towards the critical state line with increasing  $q^*$

(b) During consolidation, a predominantly horizontal line with increasing  $p'$ , thus moving away from the critical state line. Slight departures from these typical patterns are seen in the initially more overconsolidated points P1 and P10, as consolida-

TEST MA3 - STAGE 3-END



EXCESS PORE PRESSURE  $\Delta u$  (kPa)

Fig. 19. Computed excess pore pressure.

tion during stage 1 at P1 was associated with increase in  $q^*$  and only marginal increase in  $p'$ , and at P10 was associated with a slight decrease in  $q^*$  while  $p'$  was held constant.

Computed stress paths indicate that all three points, P1, P10, and P11, initially at the overconsolidated state reach yielding conditions during stage 2 of construction; point P11, the least overconsolidated of the three, started yielding in lift 1, but P1 and P10, both at initial  $K_0$  conditions very close to unity, reached yield conditions in lift 2. Most of the clay foundation under the embankment was also at a normally consolidated state at the end of stage 2, which explains why both computed and measured deformations increased more rapidly following completion of lift 3 loading.

At points P8, P10, and P11 under the embankment slope, stress paths moved very close to the critical state line, particularly on completion of stages 3 and 5 loading. At points P2 and P7, located at greater depths, stress paths during loading

were predominantly vertical and never approached the critical state line.

**Conclusions**

A coupled consolidation numerical analysis of a stage-constructed embankment test has been presented adopting the modified Cam-clay model for the clay foundation. Soft clay parameters were obtained from the large amount of test data available. No calibration of parameters was carried out. Values of shear modulus  $G$  were made dependent on the mean effective stress  $p'$  and values of permeability were related to the void ratio, as these more realistic assumptions appear to be important in the case of a stage-constructed embankment.

Good overall agreement of maximum magnitudes of horizontal and vertical displacements and of pore pressure variation with time has been obtained. Agreement was particularly promising for settlements at the ground surface under the embankment and for pore pressure generation and dissipation: the kaolin clay.

Agreement was less satisfactory for displacements at greater depths, where both horizontal and vertical displacements were overpredicted. Shapes of computed and measured lateral deformation profiles with depth were also different. Some reasons for the differences are the modelling of the embankment as a linear elastic material and that anisotropy of the clay foundation was not considered in the modified Cam-clay model.

Because of the general good agreement obtained in this well-controlled centrifuge experiment, and indeed with other field cases reported in the literature, the numerical model adopted here is recommended for practical applications of embankments on soft clays.

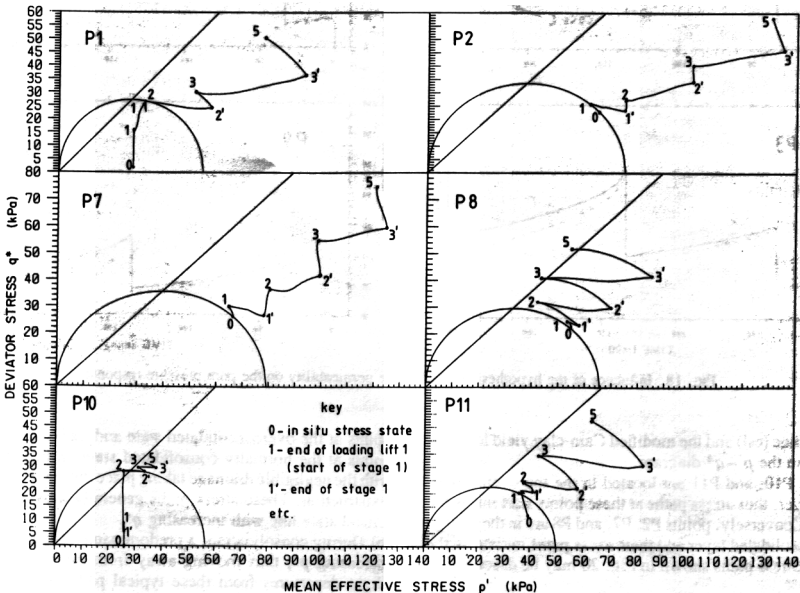


Fig. 20. Computed stress paths at the location of transducers P1, P2, P7, P8, P10, and P11.

### Acknowledgements

The research reported here has been partly funded by a contract with the Corps of Engineers, U.S. Army, European Research Office. Financial support to the first author was provided by the Brazilian Research Council (CNPq) and Federal University of Rio de Janeiro (UFRJ). Thanks are also due to the technical staff of the Soils Group at the Engineering Department, Cambridge University, for support provided during the centrifuge tests.

- AIREY, D. 1984. Clays in circular simple shear apparatus. Ph.D. thesis, Engineering Department, Cambridge University, Cambridge, England.
- ALMEIDA, M. S. S. 1981. Analysis of the behaviour of an embankment on soft clay. M.Phil. thesis, Engineering Department, Cambridge University, Cambridge, England.
- 1984. Stage constructed embankments on soft clays. Ph.D. thesis, Engineering Department, Cambridge University, Cambridge, England.
- ALMEIDA, M. S. S., and ORTIGÃO, J. A. R. 1982. Performance and finite element analysis of a trial embankment on soft clay. Proceedings of the International Symposium on Numerical Models in Geomechanics, Zurich, Switzerland, pp. 548–558.
- ALMEIDA, M. S. S., and PARRY, R. H. G. 1985. Centrifuge studies of embankment foundations strengthened with granular columns. Third NIT International Geotechnical Seminar, Singapore, pp. 153–163.
- ALMEIDA, M. S. S., DAVIES, M. C. R., and PARRY, R. H. G. 1985. Centrifuge embankments on strengthened and unstrengthened clay foundations. *Géotechnique*, 35(4), pp. 425–441.
- BASSETT, R. H., DAVIES, M. C. R., GUNN, M. J., and PARRY, R. H. G. 1981. Centrifugal models to evaluate numerical methods. Proceedings, International Conference on Soil Mechanics and Foundation Engineering, Stockholm, Sweden, Vol. 1, pp. 557–562.
- CHAN, K. C. 1975. Stresses and strains induced in soft clay by a strip footing. Ph.D. thesis, Engineering Department, Cambridge University, Cambridge, England.
- DAVIDSON, C. S. 1980. The shear modulus of clays, Part II. Research project, Cambridge University, Cambridge, England.
- DAVIES, M. C. R. 1981. Centrifugal modelling of embankments on clay foundations. Ph.D. thesis, Engineering Department, Cambridge University, Cambridge, England.
- DAVIES, M. C. R., and PARRY, R. H. G. 1985. Centrifuge modelling of embankments on clay foundations. *Soils and Foundations*, 25, pp. 19–36.
- GIBSON, R. E., KNIGHT, K., and TAYLOR, P. W. 1963. A critical experience to examine theories of three dimensional consolidation. Proceedings, European Conference on Soil Mechanics and Foundation Engineering, Weisbaden, West Germany, Vol. 1, pp. 69–76.
- GUNN, M. J., and BRITTO, A. M. 1981. CRISP—User's and programmer's manual. Engineering Department, Cambridge University, Cambridge, England.
- HOULSBY, G. T. 1981. A study of plasticity theories and their applicability to soils. Ph.D. thesis, Engineering Department, Cambridge University, Cambridge, England.
- JAMES, R. G. 1973. Determination of strains in soils by radiography. CUED/C SOILS LNI(a), Engineering Department, Cambridge University, Cambridge, England.
- KAVAZANJIAN, E., and POEPEL, P. H. 1984. Numerical analysis of two embankment foundations. Proceedings, ASCE Symposium on Sedimentation Consolidation Models, San Francisco, CA, pp. 84–106.
- MAGNAN, J. P., HUMBERT, P., BELKEZIZ, A., and MOURATIDIS, A. 1982a. Finite element analysis of consolidation, with special reference to the case of strain hardening elastoplastic stress-strain models. Proceedings, IV International Conference on Numerical Methods in Geomechanics, Edmonton, Alta., pp. 327–336.
- MAGNAN, J. P., HUMBERT, P., and MOURATIDIS, A. 1982b. Finite element analysis of soil deformations with time under an experimental embankment at failure. Proceedings, International Conference on Numerical Models in Geomechanics, Zurich, Switzerland, pp. 601–609.
- NAYLOR, D. J. 1975. Non-linear finite elements for soils. Ph.D. thesis. Department of Civil Engineering, University College of Swansea, Swansea, United Kingdom.
- PARRY, R. H. G., and NADARAJAH, V. 1973. Observations in laboratory prepared lightly overconsolidated kaolin. *Géotechnique*, 24, pp. 345–357.
- PARRY, R. H. G., and WROTH, C. P. 1977. Shear properties of soft clays. Report presented at Symposium on Soft Clay, Bangkok, Thailand.
- POULOS, H. G. 1972. Difficulties in prediction of horizontal deformations of foundations. *ASCE Journal of the Soil Mechanics and Foundations Division*, 98(SM8), pp. 843–848.
- ROSCOE, K. H., and BURLAND, J. B. 1968. On the generalized behaviour of 'wet' clay. In *Engineering plasticity*. Edited by J. Heyman, and F. Leckie. Cambridge University Press, London, England, pp. 535–609.
- SCHOFIELD, A. N. 1980. Cambridge geotechnical centrifuge operations. *Géotechnique*, 30(3), pp. 227–268.
- SCHOFIELD, A. N., and WROTH, C. P. 1968. Critical state soil mechanics. McGraw-Hill, London, England.
- SIMPSON, B. 1973. Finite element computations in soil mechanics. Ph.D. thesis, Engineering Department, Cambridge University, Cambridge, England.
- SMALL, J. C., BOOKER, J. R., and DAVIS, E. H. 1976. Elastoplastic consolidation of soil. *International Journal of Solids and Structures*, 12(6), pp. 431–488.
- TAVENAS, F. 1981. Some aspects of clay behaviour and their consequences on modelling techniques. American Society for Testing and Materials, Special Technical Publication No. 740, pp. 667–677.
- THOMPSON, S. A. 1976. Application of finite elements to plane strain deformation and consolidation of soils. Ph.D. thesis, Engineering Department, Cambridge University, Cambridge, England.
- THOMPSON, W. J. 1962. Some deformation characteristics of Cambridge Gault clay. Ph.D. thesis, Engineering Department, Cambridge University, Cambridge, England.
- TRUONG, D. M., and MAGNAN, J. P. 1977. Application des modèles élastoplastiques de l'Université de Cambridge au calcul du comportement d'un remblais expérimental sur sols mous. *Laboratoire Central des Ponts et Chaussées, Rapport de Recherche LPC No. 74*.
- WOOD, D. M. 1982. Choice of models for geotechnical predictions. Technical Report CUED/D-SOILS TR126. Engineering Department, Cambridge University, Cambridge, England.
- WROTH, C. P. 1977. The predicted performance of soft clay under a trial embankment loading based on the Cam-clay model. In *Finite elements in geomechanics*. Edited by G. Gudehus. John Wiley & Sons, Chapt. 6, pp. 191–208.
- WROTH, C. P., and SIMPSON, B. 1972. An induced failure of a trial embankment: part II finite element computations. Proceedings, Conference on the Performance of Earth and Earth Supported Structures, American Society of Civil Engineers, pp. 65–79.

### List of symbols

$e_{cs}$	void ratio at critical state line at $p' = 1 \text{ kPa}$
$k_h, k_v$	permeability in the horizontal and vertical directions
$p'$	mean normal effective stress = $(\sigma'_1 + \sigma'_2 + \sigma'_3)/3$
$p'_c$	isotropic preconsolidation pressure
$p'_o$	mean <i>in situ</i> effective stress = $(\sigma'_{vo} + 2\sigma'_{ho})/3$
$q^*$	generalized deviator stress = $[(\sigma'_1 - \sigma'_2)^2 + (\sigma'_2 - \sigma'_3)^2 + (\sigma'_1 - \sigma'_3)^2]^{1/2}$
$t$	time
$u$	pore-water pressure
$z$	depth
$C_c$	gradient of the compression line in the $e - \log p'$ plot

$C_s$	gradient of the swelling line in the $e - \log p'$ plot	OCR	overconsolidation ratio ( $\sigma'_{vm}/\sigma'_{vo}$ )
$C_k$	slope of the $e - \log k_v$ line	$\kappa$	gradient of the swelling line in the $e - \ln p'$ plot
$E$	Young's modulus	$\lambda$	gradient of the compression line in the $e - \ln p'$ plot
$G$	shear modulus	$\nu'$	Poisson's ratio in terms of effective stress
$H$	total depth of the clay foundation	$\sigma'_1, \sigma'_2, \sigma'_3$	principal effective stresses
$K'$	bulk modulus in terms of effective stress	$\sigma'_h, \sigma'_v$	horizontal and vertical effective stresses
$K_o$	coefficient of lateral earth pressure at rest	$\sigma'_{ho}, \sigma'_{vo}$	<i>in situ</i> horizontal and vertical effective stresses
$K_{rc}$	coefficient of lateral earth pressure at rest in the normally consolidated condition	$\sigma'_{vm}$	maximum vertical effective stress
$N$	gravity scaling factor (centrifuge acceleration $Ng$ )	$\Delta u$	excess pore pressure
		$M$	critical state frictional constant